Appl. Phys. A 49, 547–562 (1989)

Applied Physics A Solids and Surfaces

Magnetic Properties of 3*d* Transition Metal Monolayers on Metal Substrates

S. Blügel*, B. Drittler, R. Zeller, and P. H. Dederichs

Institut für Festkörperforschung der Kernforschungsanlage Jülich, D-5170 Jülich, Fed. Rep. Germany

Received 29 April 1989/Accepted 13 June 1989

Abstract. We report results of systematic calculations for magnetic properties of 3*d* transition metal monolayers on Pd(001) and Ag(001). We find large similarities to interactions of magnetic 3*d* impurities in the bulk. Therefore the overlayer results are supplemented with results for 3*d* dimers in Cu, Ag, and Pd. Differences between the two classes of systems are utilized to reveal the interaction within the overlayers and between overlayers and substrates. In virtually all cases we find both ferromagnetic and antiferromagnetic solutions, showing large magnetic moments and similar densities of states. From the trend of the calculations we conclude that V, Cr, and Mn overlayers favor the antiferromagnetic c(2 × 2) structure, while Ti, Fe, Co, and Ni prefer the ferromagnetic one.

PACS: 75.30Pd, 75.70Ak

Recent experimental studies [1–3] signal considerable activity in exploring the frontier field of ultrathin magnetic films. Theoretical predictions of magnetic overlayers and interlayers [4–7] with greatly enhanced moments played a crucial role in motivating and guiding the experimental realizations of two dimensional (2D) models exhibiting itinerant magnetism. Whereas previous experimental findings were entirely explained in terms of ferromagnetism we found recently [8] that V, Cr, and Mn monolayers on the Pd(001) substrate order in a c(2 × 2) antiferromagnetic superstructure. From strong analogies to the interaction of corresponding 3*d* impurity dimers in Cu and Ag [9] we conjectured that this antiferromagnetic ordering of V, Cr, and Mn monolayers (ML) and the ferromagnetic one of Fe, Co, and Ni monolayers should be a universal behavior on the (001) surfaces of Pd, Pt, and the noble metals. This conjecture is in line with results for Cr on Au(001) [10] and has been confirmed in recent extensive calculations for 3*d* overlayers on Ag(001) [11]. Qualitatively this is also in line with calculations for isolated Mo monolayers [12, 13] for which the antiferromagnetic solution is found to be most stable. However, it is in contradiction with previous theoretical results for 3*d* metal monolayers which predict ferromagnetism also for the early 3*d*-metal systems [4, 5], basically because in these calculations the antiferromagnetic state has not been examined.

Experimentalists have recently acquired great sophistication in manufacturing single crystal epitaxial films showing layer by layer growth and absence of interdiffusion [2], thus allowing a direct comparison with theoretical predictions. This is in particular true for noble metal substrates on which a large variety (e.g. Ni/Cu [3], Co/Au [14], Fe/Ag [15], Fe/Au [1, 2], Mn/Ag [16, 17], Cr/Ag [18], V/Ag [16, 19]) of 3*d* metals at one monolayer range has been stabilized, some of them even in non-thermodynamic phases (e.g. Co/Cu [2, 3] and Fe/Cu [1–3, 20]). Although the prediction of enhanced magnetic moments is experimentally not yet completely confirmed, the controversy on "dead" magnetic Fe and Ni layers is settled and a wide consensus between experiment and theory has been reached on the ferromagnetism of Fe, Co, and Ni

* Present address: ISSP, University of Tokyo, 7-22-1 Roppongi, Minato-ku, Tokyo 106, Japan

overlayers not only on noble metals but for instance also on the Pd substrate [21]. However, the experimental results on magnetism of the early 3*d* transition metals are very controversial indeed and do not allow one to discriminate between the different theoretical predictions made in [4, 5] and [8, 10, 11]. While recent experiments of Stampanoni et al. [22] using spin-polarized photoemission on monolayer-range ultrathin films of V/Ag(001) demonstrate the absence of ferromagnetism for this system and Moodera and Meservey [23] found for quench-condensed V atoms on Ag and Au antiferromagnetic coupling for coverages >0.03 ML and predominately a ferromagnetic one for coverages >1.5 ML, previous experiments of V on Ag(001) [19], V/Ag(111), and Mn/Ag(111) [16] had been interpreted in terms of ferromagnetism of the overlayer. Johnson et al. [24] have performed polarized neutron reflection measurements for Ag/Cr/Ag(001) sandwich structures with Cr coverages of 0.33 ML and 3.3 ML. For the 0.33 ML coverage, data suggest a long range ferromagnetic order with enhanced magnetic moments, whereas for a 3.3 ML thick layer no ferromagnetism was detected. Support for our predictions comes from transition-metal Pt alloys in the tetragonally ordered CuAu I structure. It is known from neutron diffraction experiments [25] that for those layered systems VPt and NiPt alloys are non-magnetic, CrPt and MnPt order $c(2\times 2)$ antiferromagnetically and FePt and CoPt are ferromagnetic.

The aim of the present paper is to review the extensive theoretical calculations performed in our group for 3*d* overlayers on Pd(001) and Ag(001). While part of the results have been published already in short communications [8, 11, 26, 27] we will give here a more comprehensive account. We concentrate in particular on the general trends on magnetism found in these calculations and discuss the importance of the 3*d*–3*d* hybridizations within the monolayers versus the effect of the interaction with the Pd and Ag substrate. The overlayer calculations are complemented with recent calculations for isolated, unsupported monolayers with atom positions constrained to the Ag(001) surface net (UML–Ag(001)) [28] as well as with improved calculations for the interaction energies of magnetic impurities in Cu, Ag, and Pd. The combination of these calculations for very different systems clearly illuminates the universality of the trends for the magnetic interactions found in these systems.

The outline of the paper is as follows. In Sect. 1 we present some technical information concerning the calculations. In Sect. 2 we discuss the results for ferromagnetic 3*d* overlayers on the Ag(001) surface. We compare with calculations for unsupported monolayers in order to see the effect of the interaction with the substrate. In addition, calculations for single impurities and impurity dimers in bulk Ag and Cu are included. A single impurity can be considered as the opposite limit of an unsupported monolayer having no monolayer interaction but only substrate interaction. The impurity dimers are in between. Both give very useful information about the importance of the hybridization between overlayer and substrate as well as within the overlayer. In Sect. 3 we review similar calculations for overlayers on Pd(001) [26]. In particular we discuss here the importance of the hybridization with the 4*d* electrons which leads to some characteristic differences between 3*d* overlayers on Ag(001) and Pd(001) despite of their overall similarities. We also comment on the induced polarization of the Pd substrate. Section 4 is devoted to antiferromagnetic overlayers forming a $c(2\times 2)$ superstructure on the (001) surface. In Sect. 5 we concentrate on the stability of this structure compared to the ferromagnetic one and discuss similar trends observed in calculations for isolated monolayers and for impurity dimers in Cu, Ag, and Pd. In Sect. 6 we summarize the results presented in this paper, discuss the limitations of our model and speculate on possible antiferromagnetic structures of monolayers on (110) and (111) substrates.

1. Some Details Concerning the Calculations

All calculations are based on density functional theory in the local spin density approximation. We use the exchange-correlation potential of von Barth and Hedin [29] but with the parameters as chosen by Moruzzi et al. [30]. All lattice parameters are chosen according to [30].

The results for the overlayer calculations are obtained with the full-potential linearized augmented-plane-wave method (FLAPW) in film geometry [31]. Nine-layer (001) films containing seven layers of Pd or Ag and one 3*d*-metal monolayer on each surface are considered. For the Pd substrate the interlayer separation between the monolayer and the Pd surface layer is assumed to be the same as in bulk Pd. For the Ag substrate we have estimated the interlayer separation according to results of a total energy analysis for the Cr/Au interlayer spacing by Fu et al. [32] to be the average of the bulk 3*d*-metal and bulk Ag one. To obtain reliable energy differences between the ferromagnetic $p(1\times 1)$ and the antiferromagnetic $c(2\times 2)$ phase, both structures are calculated with the same antiferromagnetic unit cell containing eighteen atoms. The symmetry properties chosen do not a priori exclude the revelation of a possible ferrimagnetic superstructure. A total number between 2×850 and 2×950 symmetrized plane waves is used as variational

basis set. We found that sufficiently accurate Brillouin-zone integrations can be performed by using ten special $k_{||}$ points [33] in the irreducible wedge of the 2D Brillouin-zone of the c(2 × 2) structure. For the p(1 × 1) structure 36 special $k_{||}$ points proved to be sufficient. Critical cases such as Ni on Ag(001) have been checked with 78 $k_{||}$ points. Lattice harmonics with angular momentum components $l \leqq 8$ are included to describe charge and potential inside touching muffin-tin spheres. All states including core states are calculated self-consistently. The calculations for the unsupported monolayers are performed by the same method with only one layer of 3*d* atoms containing two atoms per unit cell.

The results for the impurities and impurity dimers are obtained with the Korringa-Kohn-Rostocker Green's-function (KKR–GF) method [34]. Starting with the Green's function of the host, as evaluated from a KKR band structure calculation, a cluster of perturbed potentials inserted into the otherwise unperturbed host is considered. The Dyson equation for the Green's function of the perturbed system, describing the multiple scattering at and within the cluster of perturbed potentials, is solved exactly. Angular momenta up to $l \leqq 3$ are taken into account and several shells of perturbed host potentials around the impurities are included. All potentials are assumed to be spherically symmetric atomic sphere potentials and are calculated self-consistently. We applied the complex energy technique [35] using 64 complex energy points. Self-consistency is accelerated by applying Broyden's method [12]. In the total energy calculations [36] the full non-sphericity of the charge density is included. However, integrals over the Wigner Seitz cell are replaced by integrals over Wigner Seitz spheres.

The local density of states (LDOS) and local magnetic moments presented in succeeding chapters are data with respect to the muffin-tin and Wigner-Seitz spheres respectively. While for the Pd substrate the volume of the overlayer muffin-tin spheres are all equal, they vary somewhat for the Ag substrate depending on the interlayer spacing chosen. For the unsupported monolayers all spheres are of equal size but larger than in the overlayer case. However, these are minor effects which do not interfere with arguments given below.

2. Ferromagnetic Overlayers on Ag(001)

Figure 1 shows the local densities of states (LDOS) of 3*d* overlayers on Ag(001) as resulting from a paramagnetic calculation. The major structure arises from the well defined *d* band of the transition metal atoms being

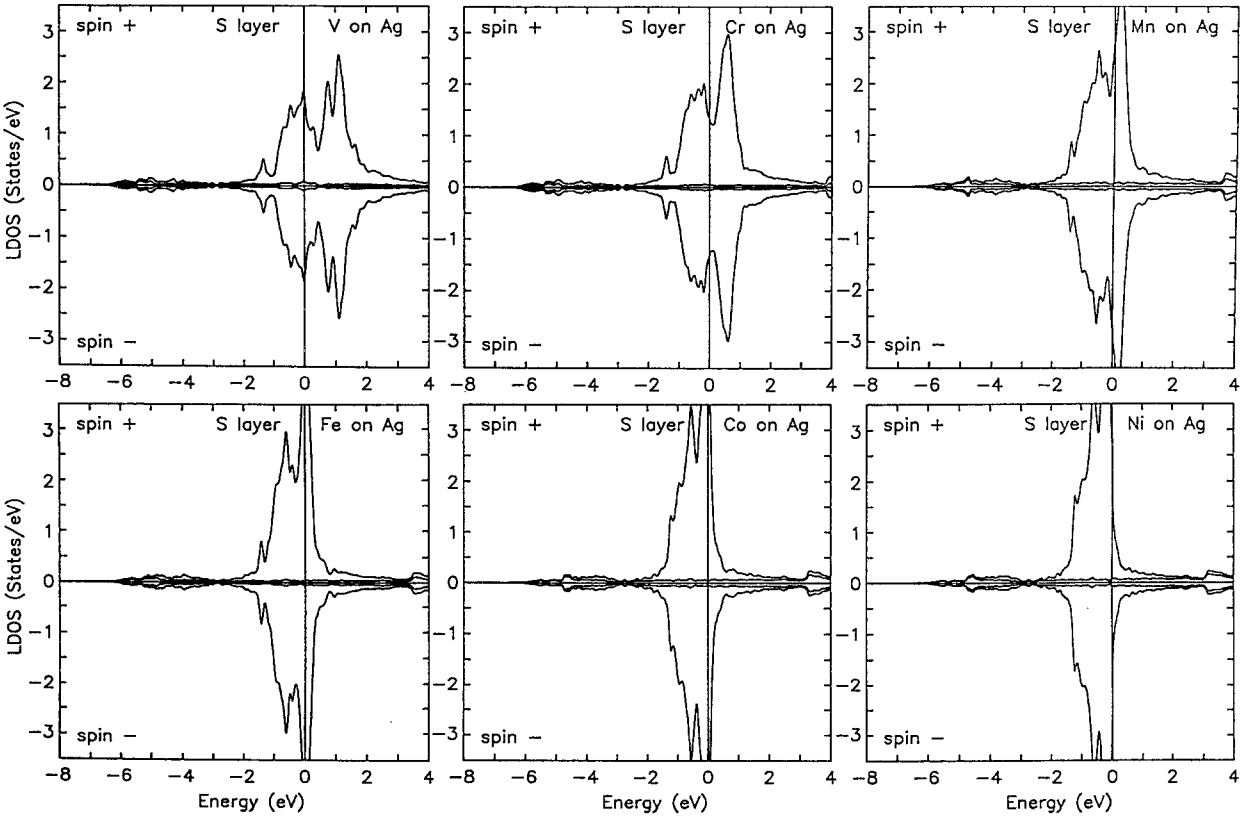

Fig. 1. Local densities of states (LDOS) of 3*d* overlayers on Ag(001) in a non-spin-polarized calculation

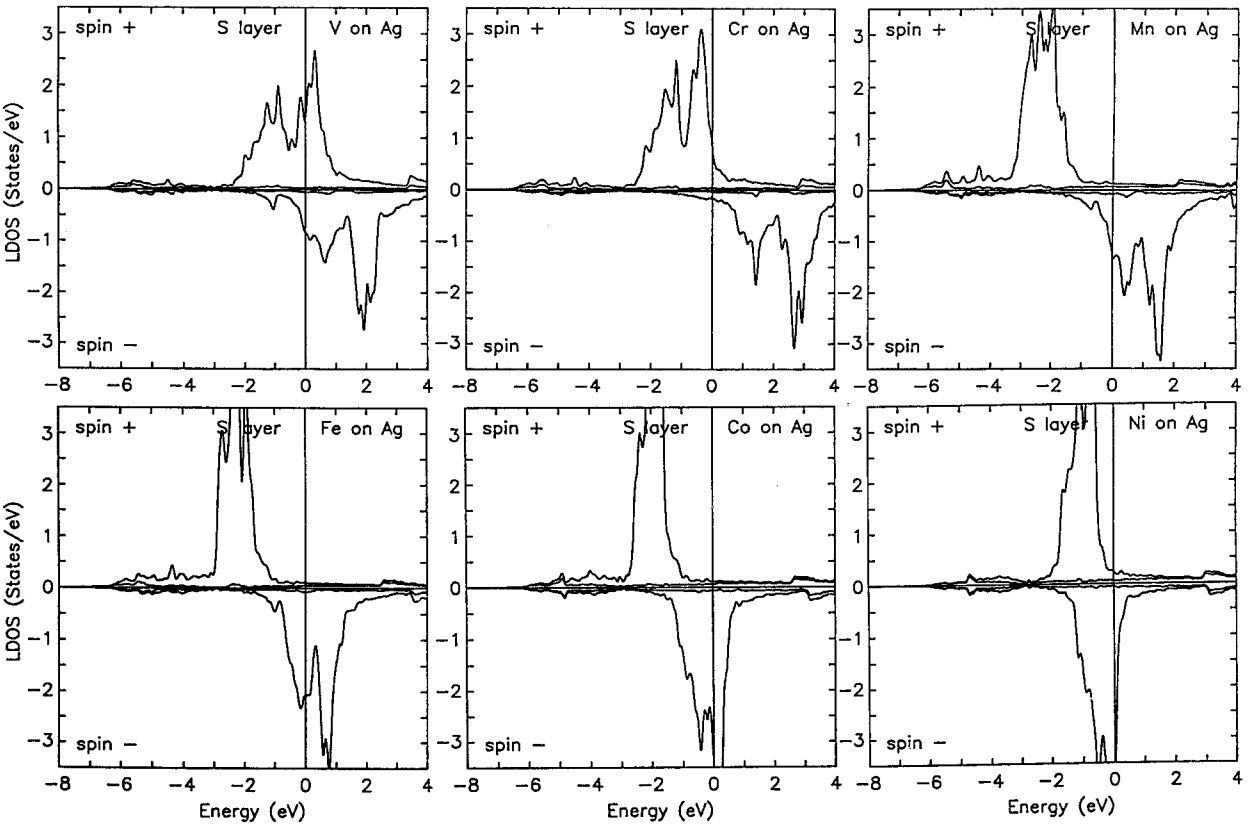

Fig. 2. LDOS of 3*d* overlayers on Ag(001) for the ferromagnetic p(1 × 1) configuration

a consequence of the 2D periodicity of the overlayer. In the sequence from V to Ni one sees a strong band narrowing. In all cases the bandwidth is substantially narrower than the corresponding metallic bulk values. This is consistent with the naive argument that a reduced coordination number will lead to band narrowing and a larger LDOS at the Fermi energy (E_F) and hence to stronger magnetism. With an exchange integral I varying from 0.7 eV at the beginning to 1 eV at the end of the 3*d* series [37] the Stoner criterium $n(E_F)I > 1$ is satisfied in all cases, even for a Ti overlayer.

Figure 2 shows the LDOS from a spin-polarized calculation for the ferromagnetic structure. Essentially one sees a spin-split LDOS as is well known from the Stoner model for the elemental ferromagnets. But compared to elemental bulk ferromagnets, the overlayer LDOS show a much larger ratio of exchange splitting to bandwidth. The Stoner model is only approximately valid which means majority and minority bands do not shift rigidly. Rather the minority band is appreciably broader than the majority one. In the case of Mn, Fe, and Co overlayers, the majority *d* band is completely filled and is nearly so for the Ni overlayer. Thus, using the familiar terminology of bulk magnetism, we can consider these overlayers as strong ferromagnets. We might even consider the Cr overlayer as a strong ferromagnet, since here the minority band is completely empty. Concerning magnetism, in a first approximation Ag can be viewed as "s metal", since the top of the 4*d* band is already 3 eV below E_F. But for Mn, Fe, and Co overlayers the exchange splitting is so large that the $3d-4d$ hybridization between monolayer and substrate cannot be avoided completely. We notice this as a perceivable *d* intensity within the range of the Ag 4*d* band between -6.5 and -3.0 eV of the majority states of these overlayers. For the Ag substrate this effect is of minor importance due to the strong localization of the 4*d* electrons and Ag is essentially non-magnetic. This is the reason why magnetism of thin films on noble metals is considered as good a experimental realization of 2D magnetism. This is in contrast to the Pd substrate where the $3d-4d$ hybridization is an important mechanism as we will see in the next section.

The resulting moments of the 3*d* monolayers on Ag(001) are shown in Fig. 3 (full line) together with the moments for the UML–Ag(001) (dotted line) [28]. The dashed line gives the local moments for 3*d* impurities in Ag, as calculated by the KKR–GF method. The moments are also collected in Table 1 together with data we will discuss in subsequent sections. The

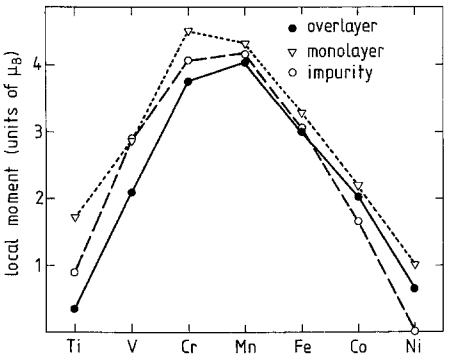

Fig. 3. Local moments for the ferromagnetic configuration of 3*d* overlayers on Ag(001) (●, full line) and of unsupported 3*d* monolayers with atomic positions constrained to the surface net of Ag(001) (UML–Ag(001)) (▽, dotted line). For comparison the local moments of 3*d* impurities in bulk Ag are also shown (○, dashed line)

isolated monolayers and single impurites in Ag can be considered as opposite idealized limits, monolayers having $3d-3d$ hybridization but no substrate hybridization and vice versa for impurities.

Figure 3 shows that all monolayers have magnetic moments substantially greater than the corresponding bulk metals. This is due to the reduced coordination number of 3*d* atoms and the large lattice constant of Ag. Both lead to narrow 3*d* bands with large LDOS at E_F and hence to large moments. The effect of a smaller lattice constant on strong ferromagnets can be seen by comparing an unsupported Ni monolayer with atomic positions fixed to the Ag(001) surface net (Ni–UML–Ag(001)) to the one having atoms fixed to the Ni(001) surface net (Ni–UML–Ni(001)). The reduction of the surface lattice constant by 14% reduces the Ni moment moderately from $1.02\mu_B$ to about $0.85\mu_B$ [38, 39] respectively. This is due to the $3d-4sp$ dehybridization. Upon reducing the lattice constant of the monolayer the Ni *sp* states hybridize more strongly with the monolayer 3*d* band, thus forming unoccupied antibonding-like hybrides above E_F. This reduces the population in the 3*d*-band and consequently the monolayer moment. The increasing *sp*-population adjusts for charge neutrality.

By comparing the moments of the overlayers and unsupported monolayers, we see that the interaction with the substrate always reduces the moments. This occurs because of the hybridization of 3*d* electrons with the 5*sp* electrons of the Ag substrate, thereby broadening the *d* density of states and reducing the tendency for ferromagnetism. However it is surprising that for Mn, Fe, and Co this effect is so small. This is a consequence of the completely filled majority *d* band of these overlayers and the corresponding monolayers. Therefore in the sequence Co, Fe, Mn the local moments increase roughly in steps of $1\mu_B$, since the population of the minority *d*-band is adjusted to satisfy charge neutrality. This is not the whole story since the number of local *sp* electrons also changes slightly by dehybridization with the Ag *sp* states and since a small charge transfer from the overlayer to the first Ag substrate layer takes place. Furthermore, the muffin-tin spheres of the UML–Ag(001) are somewhat larger than the overlayers one. In any case these are all relatively small effects, so that in the end the filling of the majority band makes it rather difficult to change the moments of the 3*d* atoms. In a sense this is a saturation effect which for practical purposes means an insensitivity of the local moments to environmental changes.

In contrast the local moments of the Cr, V, and Ti monolayers are drastically reduced upon adsorption. The Ti moment in particular is nearly wiped out. The absence of strong ferromagnetism together with the larger extent of the 3*d* wave functions leading to larger $5sp-3d$ and $3d-3d$ hybridization are responsible for these drastic changes.

Ni overlayers can be considered the opposite limit, having magnetism stabilized by 3*d* holes rather than electrons. The main difference though, is that the 3*d* wave functions for Ni are much more localized than the 3*d* wave functions of the early transition metals. The *sp* hybridization with some of those 3*d* states leads to 3*d* antibonding states which are broadened and shifted above the 3*d* band edge of Ni [40, 41]. This effect is controlled by the depth of the *sp*-band. The result of it can be seen as a small tailing off of the LDOS of Ni on Ag at E_F (Fig. 1). This reduces the moments of an Ni–UML–Ag(001) from $1.02\mu_B$ to $0.65\mu_B$ for a Ni monolayer on Ag(001) and analogously for Ni on Cu(001) from $0.87\mu_B$ [42] to $0.40\mu_B$ [38]. For Ni on Cu(111) no magnetism is expected [41].

Due to the work of Fu et al. [4] and Richter et al. [5] it has become well established that the overlayer moments are much larger than the moments of the elemental 3*d* metals. When the 3*d* overlayer moments are compared with the impurity moments as is done in Fig. 3 we find a surprising similarity as far as the general trend and the magnitude of the moments are concerned. Thus despite the very different environment which a 3*d* atom sees as an impurity in the bulk and as an adsorbed monolayer atom on the substrate, the effective hybridization with the neighboring atoms is so strongly reduced that as a consequence the moments are similar.

A second look at Fig. 3 reveals that there are also some systematic differences between the local moments of the overlayers and of the impurities. The moments in the overlayers are larger than the impurity moments for Co and Ni, but smaller than these in the case of Cr, V, and Ti. We interpret this as a direct effect

Table 1. Local moments for the 3*d*–Ag system. Given are the local moments within the muffin-tin sphere for an unsupported (001) monolayer (M_{UML}) fixed within the lattice constant of Ag, for a 3*d*-overlayer (M_{OL}) on Ag(001), for an impurity (M_I) in bulk Ag and for a 3*d*-atom of an impurity dimer (M_{ID}) on n.n. sites in Ag. The superscripts F and AF refer to the ferromagnetic and antiferromagnetic configuration. The last three lines refer to the moments of single impurities and impurity dimers in Cu

	Ti	V	Cr	Mn	Fe	Co	Ni
M^F_{UML}	1.72	2.87	4.50	4.32	3.29	2.20	1.02
M^{AF}_{UML}	0	2.59	4.09	4.32	3.32	2.10	0
M^F_{OL}	0.34	2.09	3.78	4.04	3.01	2.03	0.65
M^{AF}_{OL}	0	2.08	3.57	4.11	3.06	?	0
M_I(Ag)	0.89	2.89	4.07	4.18	3.05	1.65	0
M^F_{ID}(Ag)	0.76	2.81	4.07	4.13	3.03	1.71	0
M^{AF}_{ID}(Ag)	0	2.69	3.99	4.14	3.05	1.66	0
M_I(Cu)	0	1.10	2.99	3.40	2.51	0.89	0
M^F_{ID}(Cu)	0	0	2.68	3.23	2.47	1.14	0
M^{AF}_{ID}(Cu)	0	0	2.76	3.24	2.37	0.67	0

of the $3d-3d$ hybridization within the overlayer which enhances the moments for Co and Ni, but decreases those of Cr, V, and Ti. This effect of the $3d-3d$ hybridization can clearly be seen in calculations for 3*d*-impurity dimers on nearest neighbor (n.n.) sites in Cu and Ag, the results of those are listed in Table 1. The strength of the $3d-3d$ hybridization increases with the delocalization of the 3*d* wave function and the reduction of the dimer bond length. Therefore the hybridization effect is stronger for dimers in Cu than for dimers in Ag and stronger for the early 3*d* metals than for the later ones. Looking at Table 1 one sees that the moment of a ferromagnetic Ti and V dimer atom in Ag is reduced compared to the single impurity case. A small reduction can also be found for the moments of Mn and Fe dimers. Contrary to this we find an increase of $0.06\mu_B$ for ferromagnetic Co dimers. This effect is much more pronounced for a Cu host. Here the moment of a ferromagnetic Co dimer increases by $0.25\mu_B$ compared to the single impurity. While Mn and Cr dimers in a Cu host give evidence of a much larger decrease than in a Ag host the effect is most evident for V. The V impurity in Cu shows a moment of $1.1\mu_B$ but is non-magnetic as dimers. Ni dimers are non-magnetic in both hosts.

This $3d-3d$ interaction discussed above is actually an effective one, renormalized by the *sp* hybridization with the host electrons. The effect of the $3d-4(5)sp$ hybridization is very strong and can be most clearly seen by comparing the moments of the 3*d* impurities in Ag with those in the Cu host. In all cases the moments in Cu are much reduced since Cu has a 12% smaller lattice constant increasing the hybridization. This has

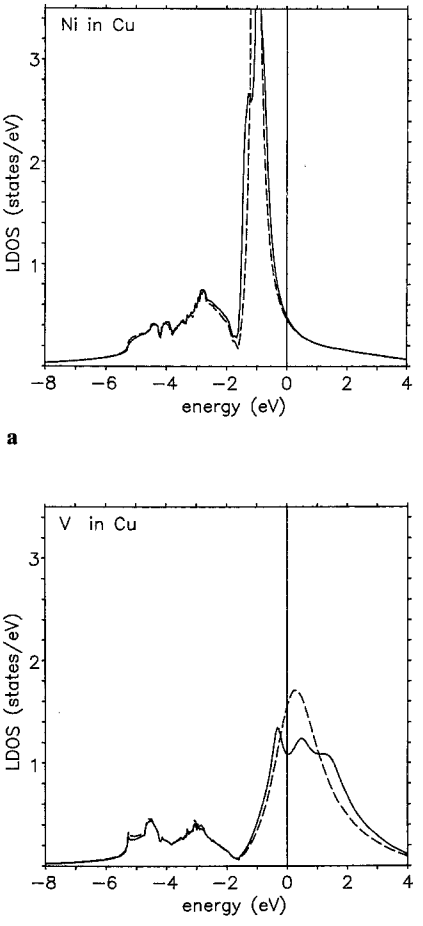

Fig. 4. a LDOS of a Ni impurity in Cu host (dashed line) and of Ni impurity dimer on nearest neighbor sites in Cu (full line). **b** LDOS of a V impurity in Cu host (non-spin-polarized calculation, dashed line) and of a V impurity dimer on nearest neighbor sites in Cu (full line)

also direct consequences for the overlayer case. Consider for instance the Fe/Ag system. For Fe on Ag(001) we found a magnetic moment of $3.01\mu_B$ and for an Fe impurity in Ag $3.05\mu_B$, showing that the effective $3d-3d$ interaction does practically not influence the moment. For an Fe impurity in Cu a magnetic moment of $2.51\mu_B$ is found, which is a reduction of $0.54\mu_B$ compared to Ag. An impurity has $12sp$ neighbors, while an overlayer atom has only 4. So we expect for Fe on Cu a moment of roughly $3.01-0.54/3=2.83\mu_B$, which is in agreement with results of Fu et al. [43] who reported $2.85\mu_B$.

In order to better understand the cooperative action of the $3d-sp$ hybridization in reducing magnetism, of the reduced coordination number in enhancing magnetism and of the *sp* renormalized $3d-3d$ hybridization in enhancing or reducing the moments, we will study the cases of Ni and V in more detail. Figure 4a shows the LDOS of a Ni impurity in Cu, which is

dominated by the well-known virtual bound state centered at 1.0 eV below E_F. Compared to a Ni impurity in Cu jellium, the peak is slighly shifted to higher energy due to the 3*d*–3*d* hybridization with the host, but with a Lorentzian shape as essentially determined by the 3*d*–4*sp* hybridization. Especially noteworthy is the high energy tail of the Lorentzian above E_F. At E_F the LDOS is already so small that the Stoner like condition for a local moment cannot be satisfied. This is contrasted by the case of a Ni overlayer (Fig. 2), where the Ni *d* band is well localized in energy and is nearly of rectangular shape. Consequently the LDOS at E_F is sufficiently high so that the Stoner condition is well satisfied. For the case of V, Fig. 4b shows the paramagnetic LDOS of a V impurity in Cu (dashed line). Since the LDOS at E_F is relatively high, the impurity is magnetic and has a moment of $1.1\mu_B$ (Table 1). However, for a V dimer in Cu (full line in Fig. 4b) the virtual bound state at E_F splits up due to the 3*d*–3*d* hybridization and the LDOS at E_F is so much reduced, that the dimer is nonmagnetic. Summarizing the case of V, we found $2.87\mu_B$ for a V–UML–Ag(001), $2.09\mu_B$ for a V monolayer on Ag(001), a further reduction for a monolayer on Ag(111) is expected, a Ag/V/Ag sandwhich with one monolayer V is reported to be non-magnetic [4] and a V monolayer on Cu is also expected to be non-magnetic.

Let us finally comment on monolayer magnetism on the Al substrate. Since the Al lattice constant is only 3% smaller than the Ag one we expect the same degree of bare 3*d*–3*d* interaction within the monolayer as for the Ag substrate, however, a much larger degree of *sp* hybridization with the substrate. Only Cr, Mn, and Fe impurities show magnetism in Al [44]. This probably remains true also for those 3*d* metals forming overlayers, whereas the magnetism of a Co monolayer on Al might show the same subtleties as Ni on Cu, with magnetism depending largely on substrate orientation.

3. Ferromagnetic Overlayers on Pd(001)

The calculated moments for ferromagnetic 3*d* overlayers on Pd(001) are shown in Fig. 5 (full line) together with the results for Ag(001) (dashed line). For the LDOS of these overlayers we refer to a recent publication [26]. The moments for the Pd overlayers are also listed in Table 2 together with the moments for 3*d* impurities and impurity dimers in bulk Pd.

Compared to the Ag substrate the overlayer moments on the Pd substrate are slightly enhanced for Ni, Co, Fe, Mn, and Cr, but strongly reduced for V and Ti. For Co, Mn, and Cr overlayers the difference is less than or about 0.1 μ_B. Since for the Co, Fe, Mn, and Cr

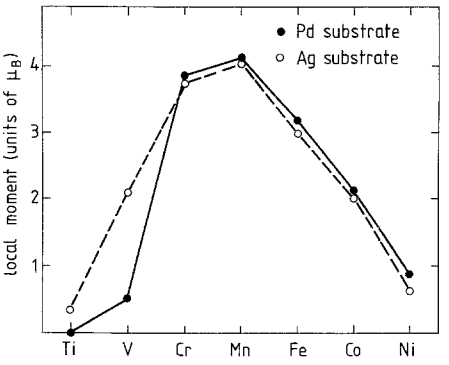

Fig. 5. Local moments of 3*d* overlayers on Pd(001) (●, full line). For comparison also the values for 3*d* overlayers on Ag(001) are given (○, dashed line)

Table 2. Local moments for the 3*d*–Pd system (the same nomenclature is used as in Table 1)

	V	Cr	Mn	Fe	Co	Ni
M_{OL}^{F}	0.51	3.87	4.11	3.19	2.12	0.89
M_{OL}^{AF}	1.39	3.46	4.05	3.20	1.99	0.59
M_i(Pd)	0	2.99	4.09	3.43	2.26	0.91
M_{ID}^{F}(Pd)	0	3.01	4.09	3.38	2.23	0.92
M_{ID}^{AF}(Pd)	0	3.00	4.05	3.39	2.22	0.87

overlayers the majority band is completely filled on both substrates (in the case of Cr one has a completely empty minority band) the substrate induced changes must be minor as explained in previous section. Therefore the changes with respect to the Ag substrate are very small. For Ni the difference is somewhat larger ($0.25\,\mu_B$) and will be discussed below.

From the electronic structure point of view there are two major differences between bulk Pd and bulk Ag: The depth of the *sp* band and even more important the position of the *d* band with respect to E_F. For Ag the upper band edge of the 3*d* band is located around 3 eV below E_F. As shown in the previous chapter the *d* electrons are well localized and insignificant for magnetic considerations. In Pd, however, the *d* band is not completely filled – about 0.36 electrons are missing – and the *d*-states are rather extended and important for magnetism. Therefore the main difference between the 3*d* monolayers on Pd(001) should arise from the strongly increased 3*d*–4*d* hybridization. One expects this to be even more important for 3*d* impurities in Pd since each impurity has 12 Pd atoms as n.n. versus 4 for a monolayer atom. Exactly this is illustrated in Fig. 6 where the calculated local moments of 3*d* impurities in Pd (full line) and in Ag (dashed line) are shown. There, the differences between the local moments show the same trend as found for the differences between the overlayers in Fig. 5, but much more pronounced. The

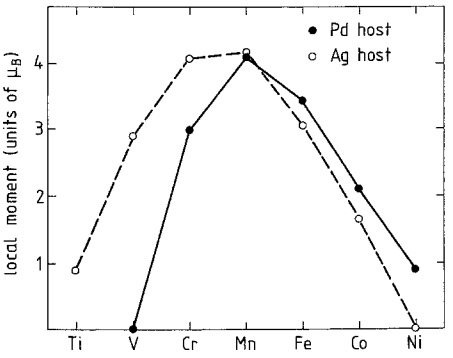

Fig. 6. Local moments of 3*d* impurities in Pd (●, full line) and in Ag (○, dashed line) host

most striking examples are V and Ni impurities, with V being magnetic in Ag bulk but remaining non-magnetic in Pd for Ni the reverse is found. Compared to Ag, the whole curve for the 3*d* impurities in Pd seems to be shifted to the right, which is essentially also what one sees in Fig. 5 for the overlayers.

To continue this line of reasoning we will discuss the LDOS of V and Ni as examples to demonstrate the effect of 3*d*–4*d* hybridization and to look into the role of 5*sp*–4*d* hybridization. Figure 7 contains the LDOS of a paramagnetic and spin-polarized calculation of a Ni impurity in Pd as well as that of the ferromagnetic Ni monolayer on Pd(001). Figure 8 shows the corresponding LDOS for the case of V. By comparing the paramagnetic LDOS of Ni in Pd with the LDOS of Ni in Cu (Fig. 4), we see dramatic differences. Due to the hybridization with the 4*d* band of Pd the Ni states are pushed up to E_F resulting in rather high LDOS at E_F so that the Stoner-like criterion for a local moment is well satisfied. Also the local band width is smaller than the one of the host resulting from the 3*d*–4*d* hybridization being reduced compared to the 4*d*–4*d* hybridization of Pd. In contrast, for V impurities in Pd the V peak is pushed high above E_F, so that the LDOS is split into bonding-like hybrides within the range of the Pd *d* band and an empty virtual bound state with antibonding character. Since the LDOS at E_F is small, the magnetic state is suppressed, and the V impurity in Pd is non-magnetic. Knowing these details from the impurity LDOS, the same trend, but much less pronounced, can also be detected for the LDOS of the overlayers. Comparing the paramagnetic LDOS of a V monolayer on Pd, which is roughly given by the average of spin up and down LDOS in Fig. 8, with the V monolayer on Ag (Fig. 1) we see that in case of the Pd substrate the LDOS is less high and more rectangular in shape. E_F is located at a small dip separating the states within the Pd band from the higher lying ones. However, the dip is not deep enough and the local moment is not suppressed, as is the case for the V impurity. The LDOS of V on Ag still shows the high

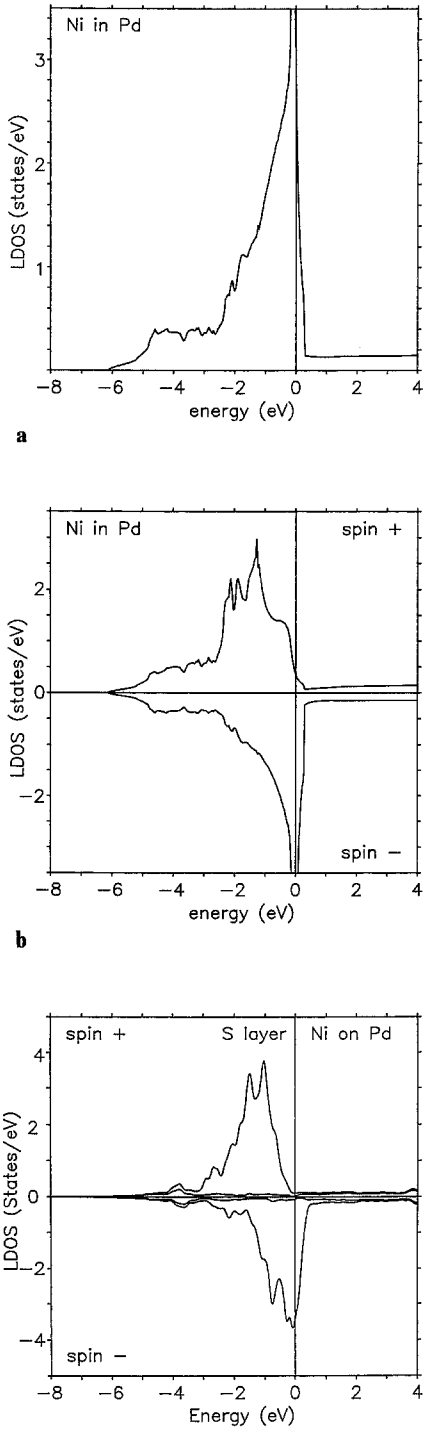

Fig. 7. a LDOS of a Ni impurity in Pd in a non-spin-polarized calculation. **b** LDOS of a Ni impurity in Pd (spin-polarized). **c** LDOS of a Ni monolayer on Pd(001) (spin-polarized)

energy *sp*–*d* hybridization tail corresponding to the tail of the Lorentzian shaped virtual bound state discussed in the previous section. This is much reduced for V on Pd and practically absent for the isolated V monolayer [28]. For a Ni monolayer on Ag this tail is already

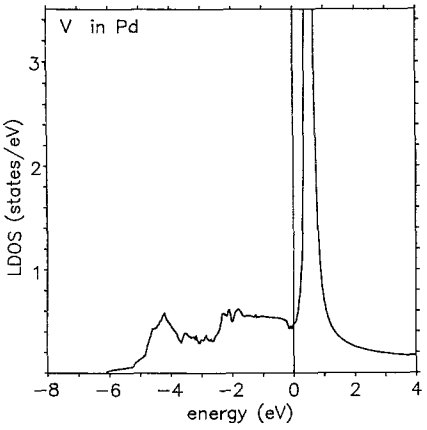

a

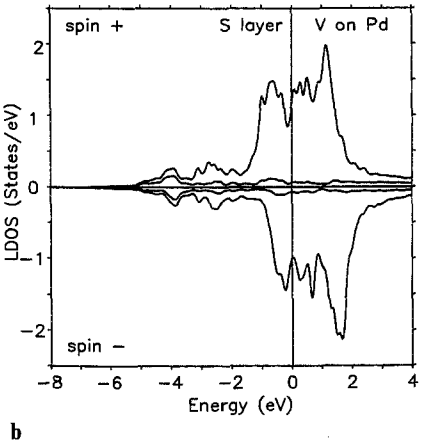

b

Fig. 8. a LDOS of a V impurity in Pd. **b** LDOS of a V monolayer on Pd(001)

fairly small, because of the increased localization of the 3*d* wave function, and negligible for Ni on Pd. Thus for these two models cases we have seen that the hybridization of the 3*d* states with the 4*d* band of Pd shifts the genuine 3*d* states of the impurities or overlayer atoms to higher energies. Also, compared to Ag, in a Pd environment the *sp* hybridization is less important. In Fig. 5 and 6 this means that the local moment curves for Pd are shifted to the right, as if the effective valence of the 3*d* atoms would be smaller in Pd than in Ag.

From the previous discussion and from the values for the local moments given in Table 2 it is apparent that the Pd and Ag systems show a different trend for the overlayer moments as compared to the impurity moments. For instance the impurity moments for Ni, Co, and Fe are larger than the overlayer moments, whereas for Cr and V the impurity moments are smaller. This result is opposite to the situation in Ag as shown in Fig. 3. The reason for this difference is that for the Pd system the 3*d*–4*d* hybridization dominates. So when one compares the impurities with the overlayers, due to the different coordination of the neighboring Pd atoms, the 3*d*–4*d* hybridization is so different, that it overwhelms the effect of the changing 3*d*–3*d* hybridization. In addition, relative to the Ag system, the role of the 3*d*–5*sp* hybridization is less important. Therefore the Ni monolayer on Pd ($0.89\mu_B$) and Ni impurity in Pd ($0.91\mu_B$) belong to the group of strong ferromagnets and can be discussed together with: Ni–UML–Ag(001) ($1.02\mu_B$), Ni–UML–Pd(001) ($0.96\mu_B$) [45], Ni–UML–Cu(001) ($0.87\mu_B$) [42], Ni–UML–Ni(001) ($0.85\mu_B$) [38], Ni(001) surface ($0.72\mu_B$) [46], and Ni bulk ($0.59\mu_B$). All these cases are strong ferromagnets with a filled majority band, but with decreasing lattice constant and increasing coordination number the moments reduce due to the *sp*–*d* dehybridization. In contrast, the Ni overlayers on Ag(001) ($0.65\mu_B$) and Cu(001) ($0.4\mu_B$) [38] are weak ferromagnets since due to the increased *sp*-hybridization the majority bands are no longer completely filled.

Due to the large spin-susceptibility of Pd one expects that the magnetic 3*d* overlayers induce sizable moments in the Pd substrate. An analogous phenomenon is well known as "giant moments" in Pd and arises from long-ranging magnetization clouds around the 3*d* impurities in Pd [47]. For the overlayers Table 3 shows the local moments M_1, M_2 of the first and second Pd layers beneath the overlayer. The moments of the inner layers, i.e. M_3 of the third layer and M_4 of the central layer are expected to be sensitiviely influenced by both overlayers whereas this is presumably a small perturbation for the first and second Pd layers. In addition, the Pd moments for these layers are quite sensitive to the values of several cut-off parameters used in the calculation and are therefore omitted from the table since they are not considered reliable enough.

With the exception of the V case, the moments in the two upper most layers couple ferromagnetically to the overlayer moment. The polarization of the top layer is very strong, i.e. far away from the weakly polarized limit discussed in Pd [47]. Bulk Pd has a *d* hole of about 0.36 electrons. For Mn, Fe, and Co overlayers the moment in the first Pd layer therefore saturates at $M_1 \cong 0.3\mu_B$. In the case of 3*d*-impurities, the first Pd shell is rather weakly polarized with an

Table 3. Induced moments M_1 and M_2 in the first and second layer of the Pd substrate. The values (in μ_B) refer to the ferromagnetic configuration of the 3*d*-monolayers M_{OL}^F on Pd(001)

	V	Cr	Mn	Fe	Co	Ni
M_1	−0.01	0.17	0.30	0.32	0.33	0.24
M_2	0.00	0.03	0.11	0.17	0.24	0.20

induced moment of $M_1 \cong 0.1\mu_B$ per Pd atom [47]. The main difference is that a Pd atom in the first layer has four 3*d* atoms as n.n., whereas a Pd atom in the first shell of an impurity has only one 3*d*-metal neighbor. Therefore the induced moments on Pd atoms in the first substrate layer are appreciably bigger.

In [47] a very simple, linear ΔZ-dependence of the induced host polarization due to 3*d*-metal impurities was found. Here ΔZ is the valence difference of the 3*d*-atom from the Ni value. Also in the overlayer case such a linear dependence of the ratio between the second and first layer moments is clearly seen. From Table 3 one finds

$$\frac{M_2}{M_1}(\Delta Z) = \left.\frac{M_2}{M_1}\right|_{\Delta Z=0} (1+0.21\Delta Z)$$

with

$$\left.\frac{M_2}{M_1}\right|_{\Delta Z=0} \cong 0.92 .$$

A similar linear relation should also exist for the third and more distant layers. To show this, self-consistency for at least 20 layers would have to be achieved, which is computationally rather impossible today. This linear relation might also be expected for the ratio between the first Pd layers and the 3*d* metal overlayers. However, the saturation effect discussed above prevents such a simple ΔZ-type behavior in the case of Mn, Fe, and Co, which means that for these systems the total magnetization is no longer strictly proportional to the overlayer magnetization. Physically, the above relation with a layer independent factor $(1+0.21\Delta Z)$ means that the spatial form of the host-polarization beyond the first layer is independent of the valence of the monolayer which determines, however, the magnitude of the polarization.

Because of the limited thickness of the film our calculations do not allow us to estimate the total moment induced in the Pd substrate. For the 3*d*-metal impurities the corresponding induced moments are known quite well, they are e.g. about $4\mu_B$ for Ni impurities, $8\mu_B$ for Co, $7\mu_B$ for Fe and $3\mu_B$ for Mn impurities [47]. Clearly for the overlayer geometry the corresponding induced moments for each 3*d*-atom should be a lot lower, basically because each overlayer atom has only four Pd neighbors to induce a moment on, so that from this simple picture one would expect a reduction by about a factor 3. In any case the above equation allows one to estimate the total magnetization of all overlayer-Pd systems if the total magnetization (at low temperatures) of one particular system has been determined experimentally.

4. Antiferromagnetic Overlayers on Ag(001) and Pd(001)

It is by no means clear whether the ferromagnetic state discussed in the previous sections is actually the ground state for the overlayers as has unconsciously been assumed in previous work [4, 5]. But in reality various antiferromagnetic states as well as noncollinear spin configurations could also play an important role. The situation is relatively simple if we assume that the magnetic interaction could be described by a n.n. Heisenberg or Ising model. Then for the square lattice of the (001) monolayer there are only two phases to worry about: the ferromagnetic $p(1\times1)$ structure discussed in previous sections and the antiferromagnetic $c(2\times2)$ superstructure shown in Fig. 9. Below we will give arguments to show that the n.n. interaction indeed dominates the behavior of the overlayers. We will therefore concentrate here on the $c(2\times2)$ antiferromagnetic structure.

Figure 10 shows the LDOS of V, Cr, Mn, and Fe overlayers on Ag(001) for this antiferromagnetic configuration. For the corresponding LDOS of V, Cr, and Mn overlayers on Pd(001) we refer to [26]. The antiferromagnetic LDOS are in first approximation similar to the ferromagnetic ones shown in Fig. 2. However, there are two important differences. Firstly the band widths are appreciably smaller, secondly there are additional small humps at the energetic positions of the main peaks, but for the opposite spin-directions. These two features are well known from the band structure of antiferromagnets [48] and can be understood by the following two step model: In the first step we allow no hybridization (hopping) between the two sublattices shown in Fig. 9. For each sublattice one then obtains a ferromagnetic band structure with an exchange splitting of $I * M$, where M is the moment, and with a band width determined by the overlap of the wave function between the n.n. sites on each sublattice. These distances however are next-nearest neighbor sites for the real $p(1\times1)$ square lattice, so that the bands are very narrow compared to the ferromagnetic ones shown in Fig. 1. In a second step we then allow

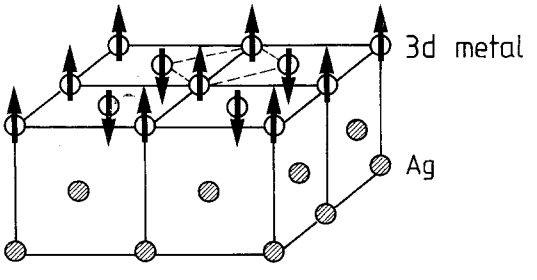

Fig. 9. The antiferromagnetic $c(2\times2)$ superstructure of the overlayer

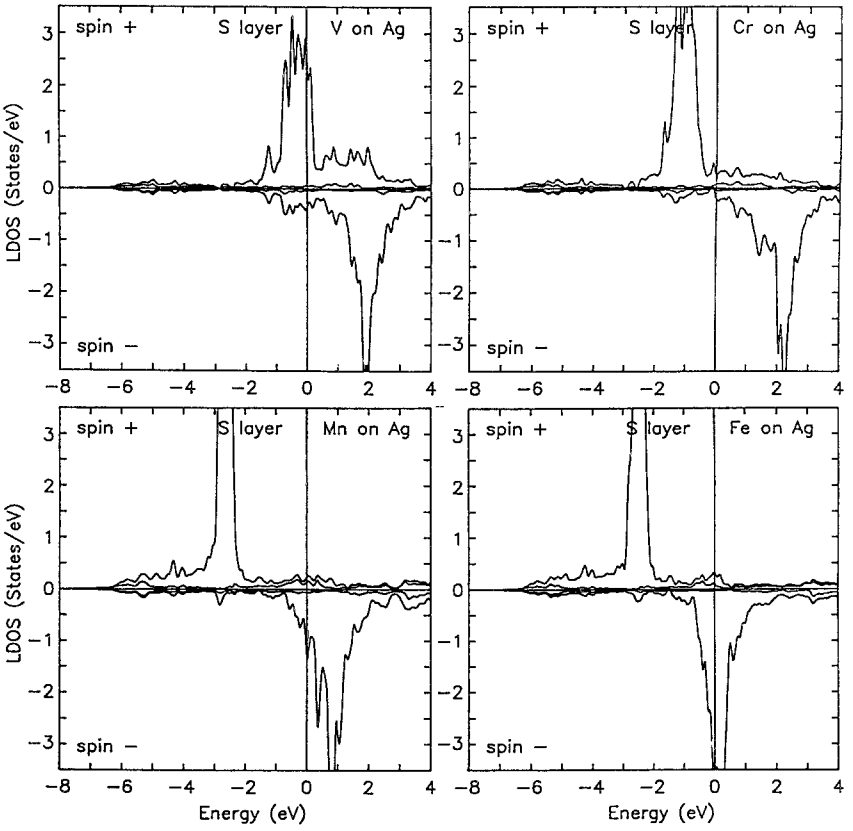

Fig. 10. LDOS of the V, Cr, Mn, and Fe monolayers on Ag(001) for the antiferromagnetic c(2 × 2) structure

hybridization between these bands of the two sublattices. Since for a given spin direction, the bands on both sublattices are due to opposite local moments centered at different energies, they covalently hybridize and produce additional humps in the LDOS at the energetic positions characteristic for the other sublattice. While these humps can be clearly recognized in Fig. 10 for the V overlayer, their intensity is quite small for Cr, Mn, and Fe as a consequence of the increasing localization of their wave functions and their larger exchange splittings.

The local moments for the antiferromagnetic c(2 × 2) phase on Ag(001) (dashed line) are shown in Fig. 11 together with the ferromagnetic moments (full line). For the Co overlayer the antiferromagnetic solution has not been calculated, the value indicated by (?) is a guess. The local moments for the antiferromagnetic configuration of the UML–Ag(001) are listed in Table 1. Also listed are the moments of the antiferromagnetic configuration of the impurity dimers. The corresponding antiferromagnetic moments for the Pd-system are given in Table 2. From Fig. 11 and from the values given in Tables 1 and 2 it becomes evident that antiferromagnetic and ferromagnetic moments have nearly the same value. This clearly shows that in almost all cases both configurations exist and are of comparable energetic stability. In most cases the antiferromagnetic moments are slightly smaller than the ferromagnetic ones. This is plausible since the additional humps in Fig. 10 have the opposite spin directions to the main peaks thus reducing their contribution to the magnetic moment. As we will show below, however, this does not mean that the antiferromagnetic solution is less stable than the ferromagnetic one, since the moment is directly connected only with the exchange energy which is only a part of the total energy.

For all three systems listed in Table 1, i.e. UML–Ag(001), the overlayers on Ag(001) and the impurity dimers in Ag, no antiferromagnetic solutions

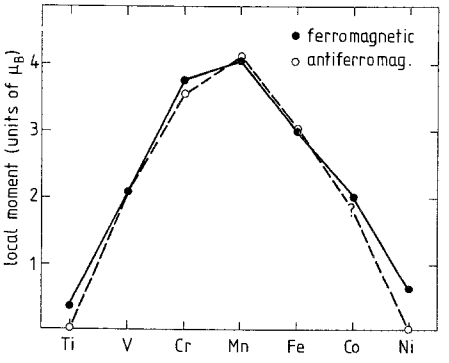

Fig. 11. Local moments of 3*d* overlayers on Ag(001) for the antiferromagnetic (o, dashed line) and the ferromagnetic structure (•, full line)

exist at the beginning and the end of the 3*d*-series, i.e. for Ti and Ni. By starting with various antiferromagnetic trial potentials in these cases the solution always converges during the iterations to the paramagnetic state $M \equiv 0$. Exceptions to this finding are the results for Pd (Table 2). Here the antiferromagnetic V overlayer has a larger moment ($1.39\mu_B$) than the ferromagnetic one ($0.51\mu_B$). As is known from bcc and fcc V-bulk calculations [49], starting from the paramagnetic solution and expanding the lattice constant slowly, the paramagnetic solution becomes instable and first the antiferromagnetic solution emerges and then for larger lattice constants the ferromagnetic one. This is analogous to results of unsupported Mo(001) monolayers [12, 13]. Apparently due to the lattice constant of Pd and its 4*d*-band position the V overlayer is in this critical regime, where the ferromagnetic state is just at the onset, but the antiferromagnetic one is already in the stable region.

5. Ferromagnetism Versus Antiferromagnetism

From the preceding discussion of the moments and LDOS, it is evident that both the ferromagnetic and the antiferromagnetic phases are more or less equally stable. Therefore a reliable total energy calculation is necessary in order to decide which configuration is the ground state and which one is a metastable one or, more likely, instable against a rotation of the local moments. The energy differences $\Delta E = E_{AF} - E_F$ per atom between the antiferromagnetic and the ferromagnetic configurations are listed in Table 4 for the 3*d* overlayers on Pd(001) and Ag(001) as well as for the UML–Ag(001), in Table 5 for 3*d* dimers on n.n. sites in Cu, Ag, and Pd. $\Delta E > 0$ (< 0) means, the ferromagnetic (antiferromagnetic) configuration is the most stable one.

Figure 12 shows the energy difference ΔE for 3*d* overlayers on Pd(001) (full line) and for 3*d* impurity dimers in bulk Pd (dashed line), Fig. 13 the corresponding results for Ag as well as for the UML–Ag(001) (dotted line). For reasons given below, the energy differences for the impurities are multiplied by a factor of two. For the overlayers on Ag and Pd a very clear trend emerges. The Ni, Co, and Fe

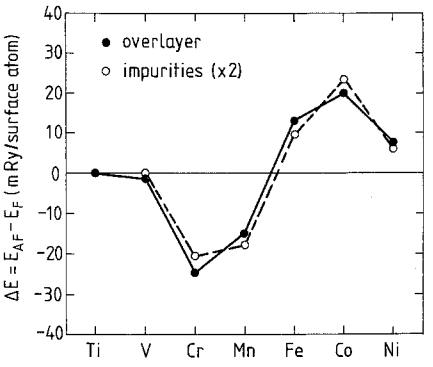

Fig. 12. Total energy difference $\Delta E = E_{AF} - E_F$ between the antiferromagnetic and the ferromagnetic configuration of 3*d* overlayers on Pd(001) (●, full line) and 3*d* impurity dimers in Pd (○, dashed line)

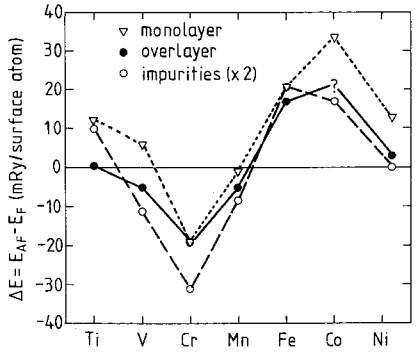

Fig. 13. Total energy difference $\Delta E = E_{AF} - E_F$ for the 3*d* overlayers on Ag(001) (●, full line), for 3*d* UML–Ag(001) (▽, dotted line) and for 3*d* impurity dimers in bulk Ag (○, dashed line)

overlayers prefer the ferromagnetic configuration and the Mn, Cr, and V ones favor antiferromagnetic ordering. For both hosts the impurity results show the same trend, which is also true for the impurity interactions in Cu (Table 5). From the strong similarities of these calculations we conclude that this is a general trend: Fe, Co, and Ni monolayers favor the p(1 × 1) ferromagnetic configuration on the (001)-surfaces of Pd, Pt and the noble metals, whereas V, Cr, and Mn monolayers prefer the c(2 × 2) antiferromagnetic one. Clearly this is the same general trend which is also known from the bulk. After all Fe, Co, and Ni are elemental ferromagnets, where as Cr and Mn prefer

Table 4. Total energy difference $\Delta E = E_{AF} - E_F$ per atom between the antiferromagnetic (AF) and ferromagnetic (F) configuration of unsupported 3*d*-monolayers and of 3*d*-overlayers on Ag(001) and Pd(001) (All values in units of mRy)

	Ti	V	Cr	Mn	Fe	Co	Ni
unsupported	+24.0[a]	+8.5	−19.1	− 1.0	+20.8	+33.9	+12.7[a]
Ag(001)	+ 0.3[a]	−5.2	−19.1	− 5.2	+16.7	?	+ 2.8[a]
Pd(001)	0	−1.5	−24.5	−15.0	+13.0	+20.1	+ 7.6

[a] Energy difference between the paramagnetic and ferromagnetic configuration

Table 5. Total energy difference $\Delta E = E_{AF} - E_F$ per atom between the antiferromagnetic and ferromagnetic configuration of 3*d*-impurity dimers on nearest neighbor sites in Cu, Ag, and Pd. (All values in mRy)

	Ti	V	Cr	Mn	Fe	Co	Ni
Cu	0	0	−27.7	−12.4	+12.8	+ 5.3	0
Ag	+4.9[a]	−5.7	−15.6	− 4.2	+10.4	+ 8.4	0
Pd	0	0	−10.3	− 8.9	+ 4.8	+11.9	+3.1

[a] Energy difference between the paramagnetic and ferromagnetic configuration

antiferromagnetic structures. This trend is even known for diatomic molecules, since Fe_2, Co_2, and Ni_2 prefer configurations with ferromagnetic coupling [50] whereas Cr_2 and Mo_2 couple strongly antiferromagnetically [51]. We will come back to a discussion of this trend below.

Firstly we will discuss the results for the overlayers and impurities in somewhat more detail. If we take the impurity interaction energies in the Ag or Pd hosts and assume a n.n. Ising model for the interaction in the overlayer, with the exchange constant fitted to the impurity interaction, we obtain for the energy difference ΔE of the overlayer the dashed curves in Figs. 12 and 13, which is just twice the energy difference for the impurity dimers. The agreement with the FLAPW calculations is quite surprising. From the close agreement with the impurity results we conclude that the n.n. interaction is the dominating driving force in the overlayer. Therefore antiferromagnetic structures other than the c(2 × 2) one are unlikely to be stable for the (001) surface. This is supported by calculations of the longer-range interaction of impurities in Cu and Ag [9] which indeed show that the n.n. interaction is the dominant one.

By comparing the impurity interactions ΔE for the Ag and Pd hosts, e.g. by plotting both curves in the same graph, we find that the Pd-curve is essentially the same as the Ag-curve, but shifted to the right. This is an effect of the strong hybridization between the overlayer 3*d*-electrons and the 4*d*-ones of Pd. As we have discussed in Sect. 3 this shifts the 3*d*-peaks to higher energies which effectively shows up as a reduced valence of the 3*d*-atoms. A similar but smaller effect can also be seen by comparing the ΔE-values for the overlayers on Pd and Ag.

The competition between ferromagnetism and antiferromagnetism has been extensively discussed by Heine and Samson [52] and Terakura et al. [53] on the grounds of stability arguments. By calculating a wave vector dependent susceptibility $\chi(\mathbf{q}, E_F)$ these authors [52, 53] find that the condition for ferromagnetism, $I * \chi(0, E_F) > 1$, is most favorably satisfied when E_F lies at the lower or upper end of the *d* band, i.e. at the beginning or the end of the 3*d* series. However, in the middle of the 3*d* series the condition for antiferromagnetism $I * \chi(\mathbf{q}_s, E_F) > 1$, where $\mathbf{q}_s$ is the wave vector of the superstructure, is easier to satisfy. This is essentially the reason why Fe, Co, and Ni overlayers prefer the ferromagnetic coupling, but V, Cr, and Mn the antiferromagnetic one. The likelihood of fulfilling the condition for ferromagnetism increases with the magnitude of the LDOS at E_F, while this is not especially important for antiferromagnetism. On the other hand, susceptibility calculations [53] indicate that a pronounced dip in the LDOS at E_F is favorable for the stability of the antiferromagnetic state. Such dips can be seen, for example, in the LDOS of 3*d* monolayers on Ag (Fig. 1), separating bonding from antibonding states. They are, however, much less pronounced for the unsupported monolayers, the band width of which are also slightly narrower [28] due to the absence of the hybridization with the substrate. Since both effects favor the ferromagnetic state, this explains why the ΔE curve for the UML–Ag(001) in Fig. 13 lies above the curve for the 3*d*-overlayers on Ag(001). Thus, effectively the interaction with the substrate, leading to a dip in the LDOS and a slight band broadening, favors the antiferromagnetic configurations. This effect is most pronounced for V. Whereas the unsupported monolayer prefers the ferromagnetic configuration, the V overlayer is antiferromagnetic on both Pd(001) and Ag(001) substrates. The latter is also true for the V impurity dimers in Pd and Ag.

A similar effect is also seen when one compares the interactions of the 3*d*-dimers in Cu with those in Ag (Table 5). For Cu the lattice constant is 12% smaller than for Ag. For this reason the 3*d*–3*d* hybridization within the dimers increases leading to a more pronounced bonding–antibonding peak in the LDOS separated by a wider and deeper dip. Since the interaction energy ΔE is dominated by the direct 3*d*–3*d* overlap an increase of the interaction energy is noticed (Table 5). This is true although the 3*d* impurity moments are much reduced when compared to the moments of 3*d* impurities in Ag (Table 1). This is due to the strongly increased 3*d*–4*sp* hybridization coming from the smaller lattice constant of Cu. Thus the smaller lattice constant of Cu campared to Ag leads to a larger exchange coupling, but broader bands and a smaller LDOS for the half-filled case. The latter two features favor the antiferromagnetic configuration. The same effect should also occur for the overlayers.

The occurrence of magnetism at the beginning of the 3*d* series is a somewhat subtle question. As it is known from the bulk, the condition for ferromagnetism $I * \chi(0, E_F) > 1$, is not met for Ti and V, so that

these elements are non-magnetic. This is due to the strongly increased 3*d* bandwidth and a decrease of the exchange integral [37]. From Figs. 1 and 2 and [26] one clearly sees that the band broadening is also very important at the beginning of the series of the 3*d* overlayers. Nevertheless we still find a ferromagnetic spin configuration for Ti on Ag(001) (with a very small moment though) as well as for Ti dimers in Ag (Table 1) whereas for these systems the antiferromagnetic configuration is suppressed. Similar things happen for V on Pd, here the ferromagnetic state is nearly suppressed while the antiferromagnetic one is retained (Table 4).

We end by commenting briefly on small structural changes. Fu and Freeman [32] performed calculations for Au/Cr/Au(001) sandwiches and found a remarkable insensitivity of the local moments to interface relaxations. This is in line with our findings that the magnetism of strong (anti)ferromagnets – Ni, Co, Fe, Mn, Cr – changes only very moderately with respect to comparatively large changes ($\sim 14\%$) of the lattice parameters. Another extreme example indicating the limited influence of relaxations are the impurity calculations for the Cu and Ag hosts. Even though the Cu lattice constant is 12% smaller than that of Ag, the overall features of the moments and the magnetic interactions are the same in both alloys. Therefore we can conclude that the self-consistent determination of the interface relaxations will not change the trends found in our calculations. Furthermore from Figs. 12 and 13 as well as Tables 4 and 5 we realize that for Cr, Fe, and Co layers the energy difference between the antiferromagnetic and ferromagnetic configuration is quite sizable (> 0.2 eV). Therefore we believe that even small structural changes such as the recently discovered (5×1) reconstruction of Fe on Cu(001) [20], do not interfere with the results given here.

6. Summary and Outlook

We have presented systematic and detailed calculations for all 3*d*-transition metals as overlayers on two particular substrates, Pd(001) and Ag(001). The overlayer results are supplemented with results for unsupported monolayers as well as results for single impurities and impurity dimers in Cu, Ag, and Pd hosts. For all systems we find large magnetic moments being a consequence of the low coordination number of 3*d* metals. For the ferromagnetic Ni, Co, Fe, and Mn overlayers the 2D majority *d* band is completely filled, leading to a pronounced insensitivity to environmental changes. The same is true for Cr overlayers, because the minority band is completely empty. We gave evidence that for the Pd system the 3*d*–4*d* interaction between overlayer and substrate is the dominant one, where as it is unimportant for the Ag system. For the Ag system the in-plane $3d-3d$ and the 5*sp* hybridization are more important. For the example of Ni systems we demonstrated the effect of *sp*–*d* dehybridization for the strong ferromagnet systems, such as the unsupported Ni monolayers, Ni on Pd(001), Ni(001) surface and Ni bulk versus the effect of *sp*–*d* hybridization due to the substrate in case of Ni on Ag(001), Ni on Cu(001), and Ni on Cu(111).

In practically all cases we find that both the ferromagnetic $p(1 \times 1)$ and the antiferromagnetic $c(2 \times 2)$ configuration exist and have similar moments and LDOS. A total energy analysis shows that on both substrates Fe, Co, and Ni order ferromagnetically, but V, Cr, and Mn antiferromagnetically. Calculations for unsupported monolayers give a similar trend, but V couples ferromagnetically. We find also strong similarities to the interaction energies of 3*d* impurity dimers in bulk Cu, Ag, and Pd. From all these calculations we conclude that the n.n. interaction is the dominating one and that V, Cr, and Mn will order antiferromagnetically and Fe, Co, and Ni ferromagnetically on the (001) surfaces of Pd, Pt, and the noble metals. According to the calculations Ti orders ferromagnetically on Ag(001) and the same might be true on Au(001). A V overlayer on Cu is presumably non-magnetic. Analogous behavior is expected for the Al(001) substrate. On Al we expect Ti, V, and Ni monolayer to be non-magnetic, Cr and Mn monolayers to order antiferromagnetically, and Fe and Co monolayers to prefer the ferromagnetic order. The basic physics is also applicable to (001) sandwich structures of transition metals with Al, Pd, Pt, and noble metals although changes of the magnetic properties at the beginning and end of the 3*d* series are likely.

For monolayers on these surfaces with different orientations, e.g. (110) and (111), the same ferro- or antiferromagnetic n.n. interaction as determined from the impurity calculations are expected to dominate. In addition for the (110) surface a second coupling constant between the second neighbors enters. Depending on the sign of this constant more complicated antiferromagnetic structures could occur. This should also happen for the (111) surfaces. Here the antiferromagnetic n.n. interaction on the triangular lattice might well lead to very complicated spin configurations such as noncollinear configurations or give rise to frustration in case of constrained spin directions. In these cases due to partial cancellation of the dominating n.n. interaction longer-range interactions might also influence the structure.

The arguments given above are strictly valid only around monolayer coverage. In the very dilute limit magnetism is no longer determined by the n.n. 3*d*–3*d*

interaction but by the Ruderman-Kittel-Kasuya-Yoshida (RKKY) interaction [9] transmitted by the substrate *sp* electrons. For V, Cr, Mn overlayers beyond one monolayer, transitions to different magnetic structures are expected, although the local n.n. 3*d*–3*d* interaction remains antiferromagnetic. For V multilayers preliminary calculations [45] indicate a $c(2 \times 2)$ ferrimagnetic structure on the surface, which likely is only a projection of the helical magnetism once proposed for similar systems [54]. Cr will change to the layered antiferromagnetic bulk structure showing topological antiferromagnetism [55] on its surface. Recent experiments of Mn(001) multilayers on Ag(001) [17] give indications for a type I antiferromagnetic structure for a tetragonal symmetry, although magnetism on Mn is a very difficult matter due to the interconnection between structure and magnetism.

For the future we consider it as a challenge to experimentally identify the predicted antiferromagnetic structures. This is not a trivial task since layer by layer growth condition is indispensible and standard spin-polarized or magnetometric methods cannot distinguish between the antiferromagnetic and the paramagnetic phase. One might hope that methods like LEED analysis at the superstructure induced extra spots [56], spin-polarized neutron reflectance at grazing angle of incidence [3], spin-polarized core-level spectroscopy [57] or an rf surface impedance method [58] might lead to a definite answer of this problem.

Acknowledgements. We are thankful to D. Pescia and M. Weinert for many stimulating discussions during the course of this work. One of us (S.B.) would like to thank K. Terakura for clarifying discussions on magnetism and H. Akai for suggestions during the early stage of this work. The calculations were performed using the full-potential linearized augmented-plane-wave program for thin films originally developed by the Northwestern group. Part of this work has been finished at the Institute for Solid State Physics, University of Tokyo. The computations were performed on the Cray X-MP computers under the auspices of the Höchstleistungsrechenzentrum (HLRZ) and the KFA Jülich.

References

1. S.D. Bader, E.R. Moog: J. Appl. Phys. **61**, 3729 (1987)
2. T. Beier, D. Pescia, M. Stampanoni, A. Vaterlaus, F. Meier: Appl. Phys. A **47**, 73 (1988)
   R. Germar, W. Dürr, J.W. Krewer, D. Pescia, W. Gudat: Appl. Phys. A **47**, 393 (1988)
3. R.F. Willis, J.A.C. Bland, W. Schwarzenacher: J. Appl. Phys. **63**, 4051 (1988)
4. C.L. Fu, A.J. Freeman, T. Oguchi: Phys. Rev. Lett. **54**, 2700 (1985)
   A.J. Freeman, C.L. Fu, S. Ohnishi, M. Weinert: In *Polarized Electrons in Surface Physics*, ed. by R. Feder, Advanced Series in Surface Physics, Vol. **1** (World Scientific, Singapore 1985)
   C. Li, A.J. Freeman, C.L. Fu: J. Magn. Magn. Mat. **75**, 201 (1988)
5. R. Richter, J.G. Gay, J.R. Smith: Phys. Rev. Lett. **54**, 2704 (1985)
6. L.M. Falicov, R.H. Victora, J. Tersoff: In *The Structure of Surfaces*, ed. by M.A. van Hove, S.Y. Tong, Springer Ser. Surf. Sci., Vol. **2** (Springer, Berlin, Heidelberg 1985)
7. K. Terakura: In *Metallic Superlattices*, ed. by T. Shinjo, T. Takada, Studies in Physical and Theoretical Chemistry, Vol. **49** (Elsevier, Amsterdam 1987)
8. S. Blügel, M. Weinert, P.H. Dederichs: Phys. Rev. Lett. **60**, 1077 (1988)
9. A. Oswald, R. Zeller, P.J. Braspenning, P.H. Dederichs: J. Phys. F **15**, 193 (1985)
   A. Oswald, R. Zeller, P.H. Dederichs: J. Magn. Magn. Mat. **54–57**, 1247 (1986)
10. A.J. Freeman, C.L. Fu: J. Appl. Phys. **61**, 3356 (1987)
11. S. Blügel, P.H. Dederichs: Europhys. Lett. (submitted)
12. S. Blügel: Ph. D. thesis, Jül. Report 2197 (1988)
13. M.J. Zhu, D.M. Bylander, L. Kleinman: Phys. Rev. B. (submitted)
14. C.H. Lee, Hui He, F. Lamelas, W. Vavra, C. Uher, R. Clarke: Phys. Rev. Lett. **62**, 653 (1989)
15. B.T. Jonker, K.-H. Walker, E. Kisker, G.A. Prinz, C. Carbone: Phys. Rev. Lett. **57**, 142 (1986)
    B. Heinrich, K.B. Urquhart, A.S. Arrott, J.F. Cochran, K. Muyrthe, S.T. Purcell: Phys. Rev. Lett. **59**, 1756 (1987)
    N.C. Koon, B.T. Jonker, F.A. Volkening, J.J. Krebs, G.A. Prinz: Phys. Rev. Lett. **59**, 2463 (1987)
    M. Stampanoni, A. Vaterlaus, M. Aeschlimann, F. Meier: Phys. Rev. Lett. **59**, 2483 (1987)
16. W. Drube, F.J. Himpsel: Phys. Rev. B **35**, 4132 (1987)
17. B.T. Jonker, J.J. Krebs, G.A. Prinz: Phys. Rev. B **39**, 1399 (1989)
18. D.A. Newstead, C. Norris, C. Binns, P.C. Stephenson: J. Phys. C **20**, 6245 (1987)
19. C. Rau, G. Xing, M. Robert: J. Vac. Sci. Technol. A **6**, 579 (1988)
20. W. Daum, C. Stuhlmann, H. Ibach: Phys. Rev. Lett. **60**, 2741 (1988)
21. U. Gradmann, R. Bergholz: Phys. Rev. Lett. **52**, 771 (1984)
    F.J.A. den Broeder, H.C. Donkersloot, H.J.G. Draaisma, W.J.M. de Jonge: J. Appl. Phys. **61**, 4317 (1987)
    H.J.G. Draaisma, F.J.A. den Broeder, W.J.M. de Jonge: J. Magn. Magn. Mat. **66**, 351 (1987)
22. M. Stampanoni, A. Vaterlaus, D. Pescia, M. Aeschlimann, F. Meier, W. Dürr, S. Blügel: Phys. Rev. B **37**, 10380 (1988)
23. J.S. Moodera, R. Meservey: (To be published)
24. A.D. Johnson, J.A.C. Bland, C. Norris, H. Lauter: J. Phys. C **21**, L899 (1988)
25. J.J.M. Franse, R. Gersdorf: In: Landolt-Börnstein, ed. by K.H. Hellwege, O. Madelung, New Series III/19a (Springer, Berlin 1986)
26. S. Blügel: Europhys. Lett. **7**, 743 (1988)
27. S. Blügel, M. Weinert, P.H. Dederichs: Physica Scripta T **25**, 301 (1989)
28. S. Blügel: To be published
29. U. von Barth, L. Hedin: J. Phys. C **5**, 1629 (1972)
30. V.L. Moruzzi, J.F. Janak, A.R. Williams: *Calculated Electronic Properties of Metals* (Pergamon, New York 1978)
31. E. Wimmer, H. Krakauer, M. Weinert, A.J. Freeman: Phys. Rev. B **24**, 864 (1981)
    M. Weinert, E. Wimmer, A.J. Freeman: Phys. Rev. B **26**, 4571 (1982)
32. C.L. Fu, A.J. Freeman: Phys. Rev. B **33**, 1611 (1986)

33. D.J. Chadi, Marvin L. Cohen: Phys. Rev. B **8**, 5747 (1973)
S.L. Cunningham: Phys. Rev. B **10**, 4988 (1974)
34. R. Podloucky, R. Zeller, P.H. Dederichs: Phys. Rev. B **22**, 5777 (1980)
P.J. Braspenning, R. Zeller, A. Lodder, P.H. Dederichs: Phys. Rev. B **29**, 730 (1984)
35. R. Zeller, J. Deutz, P.H. Dederichs: Solid State Commun. **44**, 993 (1982)
36. B. Drittler, M. Weinert, R. Zeller, P.H. Dederichs: Phys. Rev. B **39**, 930 (1989)
37. J.F. Janak: Phys. Rev. B **16**, 255 (1977)
O. Gunnarsson: J. Phys. F **6**, 587 (1976)
38. D.S. Wang, A.J. Freeman, H. Krakauer: J. Appl. Phys. **52**, 2502 (1981); Phys. Rev. B **24**, 1126 (1981)
A.J. Freeman, D.S. Wang, H. Krakauer: J. Appl. Phys. **53**, 1997 (1982)
D.S. Wang, A.J. Freeman, H. Krakauer: Phys. Rev. B **26**, 1340 (1982)
39. J. Noffke, L. Fritsche: J. Phys. C **14**, 89 (1981)
40. K. Terakura: J. Phys. F **7**, 1773 (1977)
41. J. Tersoff, L.M. Falicov: Phys. Rev. B **26**, 6186 (1982)
42. Estimated by linear interpolation which is suggested in [38]
43. C.L. Fu, A.J. Freeman: Phys. Rev. B **35**, 925 (1987)
44. P.H. Dederichs, H. Akai, S. Blügel, R. Zeller: *Electronic Structure and Magnetic Properties of Impurities in Metals, Nato-Advanced Study Institute on "Alloy Phase Stability"*, Maleme (Martinus Nijhoff 1987)
45. S. Blügel: Unpublished results
46. E. Wimmer, A.J. Freeman, H. Krakauer: Phys. Rev. B **30**, 3113 (1984)
47. A. Oswald, R. Zeller, P.H. Dederichs: Phys. Rev. Lett. **56**, 1419 (1986)
48. J. Kübler: J. Magn. Magn. Mat. **20**, 277 (1980)
T. Oguchi, A.J. Freeman: J. Magn. Magn. Mat. **46**, L1 (1984)
49. K. Terakura: Private communication
50. J. Harris, R.O. Jones: J. Chem. Phys. **70**, 830 (1979)
51. B. Delley, A.J. Freeman, D.E. Ellis: Phys. Rev. Lett. **50**, 488 (1983)
J. Bernholc, N.A.W. Holzwarth: Phys. Rev. Lett. **50**, 1451 (1983)
52. V. Heine, J.H. Samson: J. Phys. F **13**, 2155 (1983)
53. K. Terakura, N. Hamada, T. Oguchi, T. Asada: J. Phys. F **12**, 1661 (1982)
54. Y. Teraoka: J. Magn. Magn. Mat. **35**, 19 (1983)
55. S. Blügel, D. Pescia, P.H. Dederichs: Phys. Rev. B **39**, 1392 (1989)
56. E. Tamura, S. Blügel, R. Feder: Solid State Commun. **65**, 1255 (1988)
57. B. Sinkovic, B. Hermsmeier, C.S. Fadley: Phys. Rev. Lett. **55**, 1227 (1985)
B. Hermsmeier, J. Osterwalder, D.J. Friedman, C.S. Fadley: Phys. Rev. Lett. **62**, 478 (1989)
58. J.S. Moodera, R. Meservey: Phys. Rev. Lett. **55**, 2082 (1985)